THE JOURNAL OF PHYSICAL CHEMISTRY C

Article

Cite This: J. Phys. Chem. C 2018, 122, 1556−1569

pubs.acs.org/JPCC

Validation of Capillarity Theory at the Nanometer Scale. II: Stability and Rupture of Water Capillary Bridges in Contact with Hydrophobic and Hydrophilic Surfaces

Alexandre B. Almeida,[†] Nicolas Giovambattista,[‡,§] Sergey V. Buldyrev,[∥] and Adriano M. Alencar*[,†]

[†]Instituto de Física, Universidade de São Paulo, 05508-090, São Paulo, São Paulo, Brazil

[‡]Department of Physics, Brooklyn College of the City University of New York, Brooklyn, New York 11210, United States

[§]Ph.D. Programs in Chemistry and Physics, The Graduate Center of the City University of New York, New York, New York, 10016 United States

[∥]Department of Physics, Yeshiva University, 500 West 185th Street, New York, New York 10033, United States

Supporting Information

ABSTRACT: We perform molecular dynamics (MD) simulations of water capillary bridges formed between parallel walls. The underlying structure of the walls corresponds to hydroxilated (crystalline) β-cristobalite, modified to cover a wide range of hydrophobicity/hydrophilicity. The capillary bridges are stretched during the MD simulations, from wall−wall separation h = 5 nm up to $h \approx 7.5$ nm, until they become unstable and break. During the stretching process, we calculate the profiles of capillary bridges as well as the force and pressure induced on the walls, among other properties. We find that, for all walls separations and surface hydrophobicity/hydrophilicity considered, the results from MD simulations are in excellent agreement with the predictions from capillarity theory (CT). In addition, we find that CT is able to predict very closely the limit of stability of the capillary bridges, i.e., the value of h at which the bridges break. We also confirm that CT predicts correctly the relationship between the surface hydrophobicity/hydrophilicity and the resulting droplets of the capillary bridge rupture. Depending on the contact angle of water with the corresponding surface, the rupture of the capillary bridges results in (i) a single droplet attached to one of the walls, (ii) two identical, or (iii) two different droplets, one attached to each wall. This work expands upon a previous study of nanoscale droplets and (stable) capillary bridges where CT was validated at the nanoscale using MD simulations. The validation of CT at such small scales is remarkable, since CT is a macroscopic theory that is expected to fail at <10 nm scales, where molecular details may become relevant. In particular, we find that CT works for capillary bridges that are ≈2-nm thick, comparable to the thickness of the water−vapor interface.

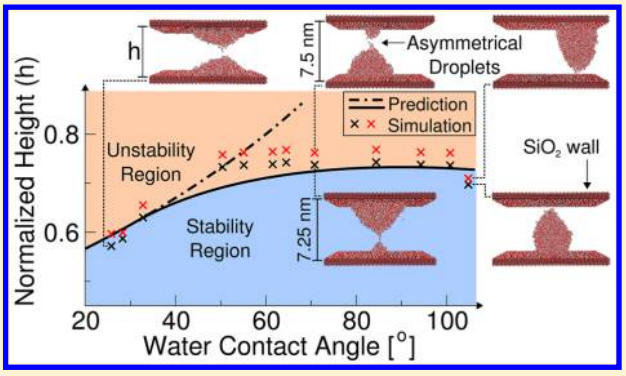

I. INTRODUCTION

Capillarity theory (CT) describes the behavior of deformable interfaces, such as the vapor−liquid interfaces in capillary bridges. CT was established in the early 19th century by Laplace and Young, who were interested in the description of the interface formed between two immiscible liquids.[1] CT is a continuum theory applicable to macroscopic systems (e.g., droplets and menisci) of dimensions much larger than typical molecular/atomic length scales. However, recent computer simulations have shown that, surprisingly, CT works for droplets and capillary bridges of nanoscale dimensions,[2] where the continuum approach could not be applied theoretically.

CT plays a fundamental role in many scientific and technological applications,[1,3] and hence extending CT to the nanoscale is of particular relevance. Capillarity phenomena can be found in different contexts. For example, capillarity affects the rearrangement of particles in liquid phase sintering,[4] and alter the transport of immiscible fluids in porous media.[5] CT has been used to explain the origin of lung pressure−volume instabilities[6−8] and crackling sound generation,[6,9] a sound associated with several lung abnormalities, during inhale[10] and exhale.[11] Examples of capillarity phenomena at the nanoscale[12] include capillary filling[13] and imbibition[14] of liquids in nanochannels, and ink-transfer processes via capillary bridges in dip-pen nanolithography.[15] In atomic force microscopy (AFM) experiments, water capillary bridges may be formed between the AFM tip and the substrate depending on the humidity conditions, affecting the measurements.[16,17] Similarly, capillary forces can also play a relevant role in the adhesion among colloidal[18] and nanoscale particles.[19]

Received: August 28, 2017
Revised: December 28, 2017
Published: December 28, 2017

DOI: 10.1021/acs.jpcc.7b08577
J. Phys. Chem. C 2018, 122, 1556−1569

Most computational studies exploring the validity of CT at the nanoscale have focused on equilibrium properties of droplets and capillary bridges.[2,20,21] Studies exploring the behavior of nanoscale capillary systems, as they become unstable, are not common and yet, these kinds of systems are of practical relevance. For example, in the case of AFM experiments, the rupture of capillary bridges formed between the AFM tip and the substrate is a process that involves a meniscus reaching its limit of stability.[22] While macroscopic CT can be applied to describe systems approaching their limit of stability, the validity of CT in this thermodynamic limits to nanoscale systems is unclear (see, e.g., ref 23).

In this work, we explore the axisymmetric capillary bridges (AS bridge) at the nanoscale by comparing the analytical solution from macroscopic CT with molecular dynamic (MD) simulation of AS bridges formed between two parallel walls. In particular, we study the behavior of AS bridges as they are stretched and become unstable. This problem is well-known and theoretical predictions can be found in the literature.[3,10] Macroscopic CT predicts that AS bridges may be stable or unstable, depending on its contact angle θ and height h.[10] As the bridge approaches the maximum height $h_{max}(\theta)$ it becomes unstable and breaks. Moreover, according to CT,[10] the outcome of AS bridges ruptures has three possible states: (i) a single droplet or (ii) two asymmetric droplets, if $\theta > 31°$, or (iii) two equal droplets, if $\theta < 31°$; where 31° is the critical contact angle. Indeed, the parameters h and θ define a phase diagram (h, θ) separating stable and unstable AS bridge, which is the subject of this work. We study the AS bridge in a wide range of θ and h, and compare the limit of stability predicted from CT with MD simulation results. In addition, for the stable AS bridge, we analyze the capillary adhesion force, Laplace pressure, contact angle, surface free energy, interface liquid–gas and liquid–solid areas, volume, and surface tension of AS bridges obtained in the MD simulations. In addition, for the unstable AS bridge, we analyze the critical height, and the size of droplets formed after the rupture. We also evaluate the fluctuation in the profile of AS bridge.

This paper is organized as follows. In section II, we describe the predictions of CT for the case of AS bridges. Namely, in section II.A, we present the analytical expressions for the profile of stable AS bridge and the forces acting on the walls, while in section II.B, we present the CT predictions regarding the stability limit of the AS bridge. In section III, we present the computer simulation details and the numerical methods employed to compare simulations versus CT. The results are presented in section IV. It consists of two parts: the study of AS bridges in the stable regime (section IV.A) and the description of AS bridges as they become unstable and break (section IV.B). A summary is included in section V.

II. CAPILLARITY THEORY OF AXISYMMETRIC CAPILLARY BRIDGES: EQUILIBRIUM PROPERTIES AND STABILITY LIMIT

In this section, we summarize the expressions from CT that describe the main properties of AS bridges. In section II.A, we present simple expressions for the properties of stable AS bridges derived from CT using the Young–Laplace equation. Equivalent expressions for the AS bridge properties can be derived from CT by minimizing the AS bridge free energy using variational calculus. These expressions are presented in the Supporting Information and summarized in section II.B. The variational calculus approach has the advantage of providing important predictions of CT regarding the AS bridge rupture, such as the maximum wall–wall separation at which the AS bridge is stable.

II.A. Axisymmetric Capillary Bridge Profile and Forces Induced on the Walls. We consider the schematic AS bridge shown in Figure 1 and provide the expressions for (i) the profile of AS bridge, as well as the (ii) force and (iii) pressure induced by the AS bridge on the walls and the (iv) surface free energy of the AS bridge.

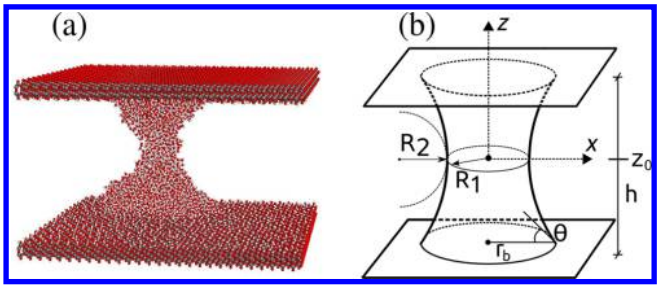

Figure 1. (a) Snapshot of a water AS bridge formed between two hydrophilic surfaces. (b) Schematic diagram of an AS bridge indicating the relevant parameters used in the present work. R_1 and R_2 are the curvature radii of the liquid–gas surface, r_b is the base radius, θ is the water contact angle, h is the walls separation, and z_0 is the neck height ($z_0 = 0$ for symmetric AS bridges). Note that R_1 is also the neck radius of the bridge, i.e., $r_0 = R_1$ in eq 2.

The profile of AS bridge is specified by the function $r(z)$ that gives the radius of the AS bridge at height z. As explained in detail in refs,[1,2] a differential equation for $r(z)$ can be obtained using Young–Laplace equation,

$$\Delta P = 2\gamma H \tag{1}$$

in which $\Delta P = P_{in} - P_{out}$, i.e., the difference of pressure inside (P_{in}) and outside (P_{out}) the AS bridge, γ is the liquid–vapor surface tension, and $H = (1/R_1 + 1/R_2)/2$ is the average curvature of the AS bridge surface (see Figure 1). It can be shown from eq 1 that the profile of stable AS bridges is given by

$$\frac{dz}{dr} = \pm \frac{|H(r^2 - r_0^2) + r_0|}{\sqrt{r^2 - [H(r^2 - r_0^2) + r_0]^2}} \tag{2}$$

where r_0 is the neck radius of AS bridge at $z = 0$, i.e., at half height of the AS bridge (r_0 is equal to the value of R_1 in Figure 1). We follow the sign convention of ref 1 where R_1 and R_2 can be positive or negative. The signs + and − in eq 2 describe, respectively, the profile of AS bridges between hydrophilic ($\theta < 90°$) and hydrophobic ($\theta > 90°$) surfaces. The analytical solution of eq 2 for $r(z)$ involves elliptic functions (see, e.g., ref 10 and the Supporting Information). However, for given values of H and r_0, eq 2 can be easily integrated numerically and the profile of AS bridge $r(z)$ predicted by CT can be calculated.

The magnitude of the net capillary adhesion force acting on the walls is given by[1]

$$F_z = F_\gamma + F_p \tag{3}$$

where

$$F_\gamma = 2\pi\gamma r_b \sin\theta \tag{4}$$

is the force on the wall due the liquid–vapor surface tension γ, and

DOI: 10.1021/acs.jpcc.7b08577
J. Phys. Chem. C 2018, 122, 1556–1569

$$F_p = -PA_{LS} = -P(\pi r_b^2) \quad (5)$$

is the force on the wall due to the pressure P within the AS bridge; $A_{LS} = \pi r_b^2$ is the area of AS bridge base. Using Young–Laplace equation and assuming $P \approx 0$ in the vapor phase, one can write $P = 2\gamma H$. Therefore

$$F_z = 2\pi r_b \gamma \sin\theta - 2\pi r_b^2 \gamma H \quad (6)$$

Note that CT only consider pressure differences between liquid and vapor phases, and the exact value of the vapor pressure is not relevant.

An equivalent equation for F_z can be obtained by noticing that the net force along the z-axis at any cross-section of the AS bridge must be constant.[1,10] Hence, if $F_{z,neck}$ is the force acting on a plane perpendicular to the AS bridge and passing through its neck (i.e., at $z = 0$), it must be that $F_{z,neck} = F_z$. The force at the AS bridge neck is given by,[1]

$$F_{z,neck} = 2\pi r_0 \gamma - 2\pi r_0^2 \gamma H = 2\pi\gamma C \quad (7)$$

where $C = r_0 - Hr_0^2$. As explained in section III, we will consider surfaces with different polarities; the surface polarity is quantified by a single parameter, k. It follows that, in the expression above, $C = C(k)$.

The pressure within the AS bridge follows from eq 3

$$P = \frac{F_\gamma - F_z}{A_{LS}} \quad (8)$$

which can be rewritten as

$$P = \frac{2\pi\gamma r_b \sin\theta - F_z}{\pi r_b^2} \quad (9)$$

The contribution of liquid–solid and liquid–vapor interfaces to the total free energy of the AS bridge is given by[10]

$$\mathcal{F} = \gamma A_{LG} + \gamma_{LS} A_{LS} + \gamma_{SG}(A_T - A_{SG}) + c \quad (10)$$

where A_{LG} (A_{SG}) is the liquid–gas (solid–gas) interface area, A_T is the total area of the walls, γ_{LG} (γ_{SG}) is the liquid–gas (solid–gas) interface tension, and c is a additive constant. Considering $c = -\gamma_{SG} A_T$ and the Young equation ($\gamma\cos\theta = \gamma_{LG} - \gamma_{LS}$), we can write $\mathcal{F}$ as

$$\mathcal{F} = \gamma(A_{LG} - \cos\theta A_{LS}) \quad (11)$$

We note that, for AS bridges at canonical ensemble, the total free energy is given by $\mathcal{F}_{total} = \mathcal{F} + \Omega\mathcal{F}_{bulk}$, where $\mathcal{F}_{bulk}$ is the free energy per unit volume of the bulk liquid and Ω is the volume of AS bridge. Since $\Omega\mathcal{F}_{bulk}$ is constant under these conditions, eq 11 also defines $\mathcal{F}_{total}$. As we will show in section IV.A, the volume of our AS bridges is practically constant, independent of h.

II.B. Limit of Stability for Axisymmetric Bridges. Closed-form expressions from CT for $r(z)$, F_z, P, $\mathcal{F}$, and other relevant quantities can be obtained as a function of the AS bridge volume Ω, contact angle θ, and walls separation h (see the Supporting Information for details). The expression for the profile of AS bridge $r(z)$, equivalent to eq 2, is given by

$$z(r) = \pm s \int_A^r \frac{dx\ (AB + x^2)}{\sqrt{(B^2 - x^2)(x^2 - A^2)}} + z_0 \quad (12)$$

for $\theta < 90°$; for the case $\theta > 90°$,

$$z(r) = \pm \int_r^B \frac{dx\ (AB + x^2)}{\sqrt{(B^2 - x^2)(x^2 - A^2)}} + z_0 \quad (13)$$

In these equations, s is the sign of the mean curvature H, z_0 is the z-coordinate of the AS bridge neck, the $\pm$ signs apply, respectively, to the portion of the AS bridge at $z > 0$ and $z < 0$ (see Figure 1), and $A > 0$ and $B \geq A$ are constants defining the shape of the profile of AS bridge. In the case of the stable AS bridge with $\theta < 90°$, $A = r_0$ is the neck radius and $B = r_b$ is the base radius. In the case of AS bridge with $\theta > 90°$, $B = r_0$ and $A = r_b$. Note that if the AS bridge is unstable, the maximum distance B will be different from r_0 or r_b.

For symmetric AS bridges ($z_0 = 0$), the quantities F_z, P, and $\mathcal{F}$ can be expressed in terms of elliptic integrals[10] that depend solely on Ω, h, and θ. Briefly, for $\theta < 90°$, F_z, P, and $\mathcal{F}$ are given by

$$F_z = \pi\gamma a \frac{h(1 - a\sin\theta)}{(1 - a^2)u(a, 1)} \quad (14)$$

$$P = 4\gamma \frac{u(a, 1)(\sin\theta - a)}{h(1 - a^2)} \quad (15)$$

and

$$\mathcal{F} \equiv \gamma\pi h^2 \frac{2\sigma(a, 1) - \cos\theta}{2u(a, 1)^2} \quad (16)$$

where $u(a, 1)$ and $\sigma(a, 1)$ are the elliptic integrals given by, respectively, eqs 2 and 7 of the Supporting Information; a is the ratio $a = A/r_b = r_0/r_b$.

For $\theta > 90°$, F_z, P, and $\mathcal{F}$ are given by the same equations, eqs 14, 15, and 16, in which a is replaced by $b = B/r_b = r_0/r_b$, and the elliptic integrals are given by eqs 31 and 32 of the Supporting Information. For stable AS bridges, we have always $r_0 < r_b$ for $\theta < 90°$, and $r_0 > r_b$ for $\theta > 90°$. Note that a and b are always related through the contact angle θ:[10]

$$(a + b)\sin\theta = 1 + ab \quad (17)$$

Parameters a ($\theta < 90°$) and b ($\theta > 90°$) are relevant to understanding the regimes of stability and instability; see the Supporting Information.

The CT predictions regarding the AS bridge rupture are relevant to this work. In particular, we note that analysis of eqs 12 and 13 indicates that there are two kinds of solutions for $z(r)$: symmetric solution, for the case $z_0 = 0$, and asymmetric solution, for $z_0 \neq 0$. According to Vogel's theorem, only symmetric profiles are stable, and the asymmetric profiles have inflection points which make the AS bridge unstable.[24,25] Analysis of the asymmetric profiles using variational calculus shows that the rupture mechanism of AS bridges depends on the contact angle θ and height h.[10] Specifically, for $\theta > 31°$, unstable AS bridges break leading to either (i) a single droplet attached to one of the walls (e.g., Figure 8a), or (ii) two droplets of different volume attached to each wall (e.g., Figure 8c). In the case $\theta < 31°$, the AS bridges break leading to two identical droplets, one on each wall (e.g., Figure 8d).

A detailed analysis of eqs 12 and 13 provides the limit of AS bridge stability with h.[10] Specifically, for $31° < \theta < 90°$ the rupture may happen symmetrically, i.e. $z_0 = 0$, at the height $h_{max,s}$, or asymmetrically, i.e. $z_0 \neq 0$, at the height $h_{max,a}$. The functions $h_{max,a}$ and $h_{max,s}$ establish, respectively, the limits of stability and metastability of the AS bridges, and are given by

DOI: 10.1021/acs.jpcc.7b08577
J. Phys. Chem. C 2018, 122, 1556–1569

$$h_{\max,a} = \left(\frac{4\Omega}{\pi\omega(a_c, 1)}\right)^{1/3} \quad (18)$$

and

$$h_{\max,s} = \left(\frac{4\Omega}{\pi\omega(a_0, 1)}\right)^{1/3} \quad (19)$$

where a_c and a_0 are the critical neck-to-base radii ratio for asymmetric and symmetric solutions, respectively.[10] They are given by equations $a_c = \tan(\theta/2)$ and

$$\left.\frac{\partial\omega}{\partial a}\right|_{a=a_0} = 0 \quad (20)$$

where $\omega(a) = v(a, 1)\, u(a, 1)^{-3}$, and $u(a, 1)$, and $v(a, 1)$ are auxiliary functions expressed in terms of Legendre elliptic integrals; see Supporting Information.

For $\theta < 31°$, $a_0 = a_c$ and hence the solution for symmetrical and asymmetrical rupture coincide $h_{\max,s} = h_{\max,a}$. For $\theta > 90°$, the rupture is only asymmetric, and the maximal stable height $h_{\max,a}$ is given by

$$h_{\max,a} = \left(\frac{4\Omega}{\pi\omega(b_c, 1)}\right)^{1/3} \quad (21)$$

where $b_c = \tan(\theta/2)$. The complete derivation of eqs 18 and 19 can be found in refs 3 and 24−27. A detailed derivation for eqs 18 and 19 is also provided in the appendix of ref 10. The Supporting Information includes the derivations of eq 21 and the main equations for $\theta > 90°$; it also includes the expressions of $r(z)$, F_z, P, and $\mathcal{F}$ for $\theta < 90°$.

III. COMPUTER SIMULATIONS AND NUMERICAL METHODS

III.A. Simulation Details. Our numerical findings are based on MD simulations of water AS bridges formed in contact between hydrophobic/hydrophilic parallel surfaces, as shown in Figure 1. The walls are perpendicular to the z-axis, located at $z = \pm h/2$, with periodic boundary conditions along the x and y directions. All simulations are performed for a cubic system of side length $L = 138.6$ Å, at constant volume, number of water molecules $N = 3375$, and temperature $T = 300$ K.

We employ the same system and methodologies used in our previous study of nanoscale water droplets and capillary bridges at fixed $h = 50$ Å.[2] A detailed description of the computer simulation techniques and methodologies can be found there. To summarize briefly, MD simulations are performed using the LAMMPS software package[28] with water molecules being represented by the SPC/E model.[29] Coulomb and Lennard-Jones interactions are cut off at distance $r_{\text{cutoff}} = 10$ Å and we calculate the long-range electrostatic interactions using a particle−particle particle−mesh solver.[30] The temperature is controlled using a Nosé−Hoover style thermostat.

We consider a family of walls that vary in the degree of hydrophobicity/hydrophilicity. These walls are described in detail in refs 31 and 32. Briefly, the walls structure corresponds to four layers of SiO_2, reproducing the (1,1,1) face of β-cristobalite. The wall surface in contact with the AS bridge is hydroxilated by attaching a H atom to each surface oxygen. The Si and O atoms are fixed during the simulation, but the OH bonds are allowed to rotate in a plane parallel to the wall. In the simulations, we measure the distance to a given wall as the distance to the plane defined by the H atoms; when $k = 0.0$, there is no H plane and we consider the plane defined by the O atoms on the surface.

All wall atoms, with exception of the H atoms, interact with water via a Lennard-Jones potential. Only the Si, O, and H atoms of the surface silanol groups have a nonzero partial charge and hence, they interact with water via Coulomb interactions. The wall structure, LJ parameters of the wall atoms, and the corresponding partial charges are provided in ref 31. In the hydroxilated β-cristobalite surface, the silanol group partial charges are $q_{0,\text{Si}} = 0.31$e, $q_{0,\text{O}} = -0.71$e, and $q_{0,\text{H}} = 0.40$e and the surface is hydrophilic, as expected. In order to vary the hydrophilicity of the surface, we follow ref 32 and rescale the silanol group partial charges by a factor $0 \le k \le 1$, i.e., $q_i \to k \times q_{0,i}$ where i = O, Si, and H. It can be easily shown that k is a dimensionless factor that quantifies the surface polarity.[32] In the case $k = 1$, one recovers the original hydroxilated surfaces.

In this present work, we are interested in the behavior of the AS bridges as the wall−wall separation increases. For a given pair of walls (defined by a specific value of k), we start the MD simulations with $h = 50$ Å. As we showed previously,[2] at this separation, CT is able to predict the profiles of AS bridges obtained in MD simulations as well as the forces on the walls induced by the AS bridge.[2] At $h = 50$ Å, the starting AS bridge configuration is a cubic configuration of water (taken from an independent simulation of bulk water at $\rho = 1$ g/cm^3 and $T = 300$ K) sandwiched by two identical surfaces. The system is simulated for $\Delta t_{\text{sim}} = 5$ ns during which the profile of capillary bridge evolves rapidly acquiring a stable and axisymmetric profile.

A sequence of simulations follows with increasing walls separations, $h = 55, 60, 65$ Å ..., until the AS bridge rupture is found. At each $h \ge 55$ Å, we run a simulation for $\Delta t_{\text{sim}} = 3$ ns. We find that, the resulting stretching rate $\Delta h/\Delta t_{\text{sim}}$ is sufficiently slow, and the stretching process of the AS bridge can be considered quasi-static. In order to prevent the premature rupture of the AS bridge when $h \to h' = h + 5$ Å, we move the walls during short 250 fs-simulations, in which each wall is displaced by 0.01 Å every 1 fs. We note that, at a given h, the termalization of the AS bridge is very fast; for example, the average forces on the walls become constant in less than 100 ps. During the simulations at a given h, the configurations of water molecules and the forces on each wall are saved every 1 ps. Only the last 2 ns of the simulated time interval Δt_{sim} are used for data analysis (see ref 2).

With the procedure described above, we identify the maximum separation h_S at which the AS bridge is stable and the critical height $h_{C'} \equiv h_S + 5$ Å at which the AS bridge rupture occurs. Since slower stretching rates may lead to smaller values of rupture height, we perform additional simulations to obtain a second estimation of the critical height h_C. Specifically, to obtain h_C, we first perform an additional simulation at $h = h_S + 2.5$ Å. If the AS bridge does not break in $\Delta t_{\text{sim}} = 20$ ns, the walls are displaced again so $h = (h_S + 2.5) + 1.25$ Å and the simulation is performed until the AS bridge breaks. As shown in section IV.B, we find that $h_S < h_{\max,a}$, while h_C and $h_{C'}$ are located around $h_{\max,a}$ and $h_{\max,s}$ (see eqs 18, 19, and 21).

III.B. Numerical Methods. Next, we describe (i) how the profiles of AS bridges are calculated from MD simulations (section III.B.1) and (ii) the procedure followed to fit these profiles (section III.B.2). We follow the same procedure employed in ref 2.

DOI: 10.1021/acs.jpcc.7b08577
J. Phys. Chem. C 2018, 122, 1556−1569

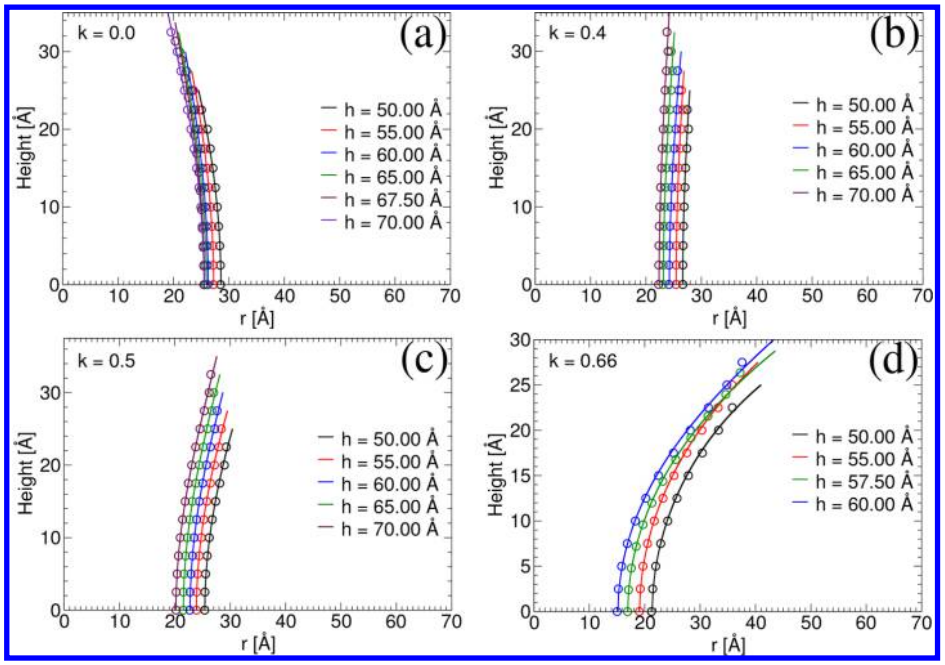

Figure 2. Average profiles of the stable AS bridges formed between walls of surface polarity k, separated by a distance h. For clarity, only the upper half of the AS bridge ($z > 0$ in Figure 1) as a function of the radius r is shown. Circles are results from MD simulations (error bars are smaller than the symbol size); solid lines are the best fits obtained from CT using eq 2. Tables 1−4 include the fitting parameters used in eq 2. Additional profiles of AS bridges, for the other values of k studied, are included in Figure S1 of the Supporting Information.

III.B.1. Profiles of Axisymmetric Bridges from MD Simulations. The profiles of AS bridges at fixed height $h \leq h_S$ are determined from 2000 water configurations saved every 1 ps during the MD simulation. The configurations are taken over the last 2 ns of the simulated time Δt_{sim}. For a given snapshot, we first define the z-axis passing through the center of mass of the AS bridge and perpendicular to the walls. The AS bridge is then covered with overlapping slabs of thickness 5 Å, parallel to the walls and shifted vertically by 2.5 Å with respect to each other. For each slab, centered at height z_i, we calculate the average density $\rho(r, z_i)$ as a function of the distance r from the z-axis. $\rho(r, z_i)$ is roughly constant within the AS bridge and it decays abruptly to practically zero in the vapor phase. Hence, we define the radius profile $r_{prof}(z)$ of AS bridge at the height $z = z_i$ as the radius at which the densities $\rho(r, z_i)$ drops from ∼1 g/cm^3 to $\rho(r, z_i) = \rho_0 = 0.2$ g/cm^3. The density $\rho(r, z_i)$ is computed using cylindrical bins of width $\Delta r = 0.5$ Å and height $\Delta z = 5$ Å. Our results are not sensitive to small changes in ρ_0. The AS bridge is symmetric with respect to its middle-height point (i.e., the AS bridge neck) located at $z = z_0 = 0$ (see Figure 1). Accordingly, we take the average of $r_{prof}(z)$ and $r_{prof}(-z)$ and report the profile only for $0 \leq z \leq h/2$.

A similar procedure is followed to calculate the profiles of unstable AS bridges ($h > h_S$). However, since at the rupture heights $h_{C'}$ and h_C the AS bridges are not necessarily symmetric, we calculate the AS bridge profile for all $-h/2 \leq z \leq h/2$, i.e., without averaging over $r_{prof}(z)$ and $r_{prof}(-z)$. In addition, since in these cases the AS bridges evolve continuously with time, we calculate the profiles in shorter time intervals of 0.1 ns. This allows us to follow the evolution of the profile of AS bridge until its rupture.

The AS bridge rupture occurs at the characteristic time τ_r, which starts to count from the moment of the last AS bridge stretching. The time τ_r is calculated from the configurations saved during the MD simulation. Specifically, for each configuration, we count the number of water molecules inside the 5 Å-slabs, and the first configuration with an empty slab defines the time τ_r at which the AS bridge breaks.

III.B.2. Profiles of Axisymmetric Bridges from Capillarity Theory. The theoretical profiles $r(z)$ of the AS bridges are obtained numerically using eq 2 by fitting the corresponding profile obtained from MD simulations $r_{prof}(z)$, where $r(z)$ is defined solely by the parameters (H, r_0). In order to identify the best fit parameters $r_{prof}(z)$, we use the following procedure: (i) On the basis of $r_{prof}(z)$, we define a range for the fitting parameters (H, r_0). We set these parameters to the corresponding lowest values to be explored, and calculate numerically the theoretical profiles $r(z)$ using eq 2. (ii) For each point (r_i, z_i) of $r_{prof}(z)$, we calculate the corresponding distance d_i to $r(z)$ [i.e., we find the line that intersects the curve $r(z)$ at a right angle and passes through (r_i, z_i), and measure the distance along this line between the intersection point on $r(z)$ and point (r_i, z_i)]. (iii) Then, we calculate the error between $r(z)$ and $r_{prof}(z)$ as

$$\epsilon = \sqrt{\frac{1}{N_p}\sum_{i=1}^{N_p} d_i^2} \tag{22}$$

where N_p is the number of points of the profile of AS bridge obtained from MD simulation. (iv) We change the parameters (H, r_0) by small increments and repeat steps ii to iv until the whole range of the parameters is covered. For each set of values (H, r_0) we obtain a value of ϵ. The set of parameters for which ϵ is minimum provides, together with eq 2, the theoretical profile of AS bridge.

We note that knowledge of the parameters (H, r_0) allows one to calculate any geometrical property of the AS bridges. For example, the contact angle for the AS bridges is obtained from the derivative of the profile given by eq 2 evaluated at $z = \pm h/2$, i.e. at one of the walls surface. Similarly, from $r(z)$, we are

DOI: 10.1021/acs.jpcc.7b08577
J. Phys. Chem. C 2018, 122, 1556−1569

Table 1. Fitting Parameters for the Profiles of AS Bridges Using Eq 2 for Heights h = 50.0 and 55.0 Å[a]

	h = 50.0 Å					h = 55.0 Å				
k	r_0 (Å)	R_2 (Å)	H (Å^{-1})	θ (deg)	ϵ (Å)	r_0 (Å)	R_2 (Å)	H (Å^{-1})	θ (deg)	ϵ (Å)
0.0	28.8	78.3	0.0238	107.1	0.03	27.5	92.7	0.0236	105.0	0.04
0.1	28.7	83.2	0.0235	106.0	0.03	27.4	96.3	0.0234	104.5	0.04
0.2	28.2	125.4	0.0217	100.4	0.03	27.1	135.3	0.0221	100.1	0.04
0.3	27.7	259.5	0.0200	94.9	0.04	26.5	404.8	0.0201	93.3	0.04
0.4	26.6	−232.8	0.0166	84.7	0.03	25.4	−249.5	0.0177	84.8	0.03
0.5	25.6	−58.8	0.0110	69.6	0.04	24.1	−61.6	0.0126	69.9	0.03
0.6	23.8	−29.8	0.0042	50.1	0.03	22.0	−31.0	0.0066	51.2	0.04
0.65	22.0	−21.7	−0.0003	34.4	0.05	19.2	−20.1	0.0012	30.8	0.07
0.66	21.4	−19.6	−0.0021	27.2	0.06	19.1	−20.0	0.0012	30.5	0.06
0.67	21.5	−19.9	−0.0018	28.4	0.05	18.2	−18.4	0.0003	25.9	0.06

[a]R_1 ($r_0 = R_1$) and R_2 are the radii of curvature of the AS bridge neck (i.e., at its middle-height point) on the x-y plane, respectively (see Figure 1). $H = \frac{1}{2}\left(\frac{1}{R_1} + \frac{1}{R_2}\right)$ is the average surface curvature of the AS bridge, θ is the contact angle, and ϵ is the error of the fitting curve from eq 22. Errors in r_0, and R_2 are ±0.05 Å.

Table 2. Same as Table 1 for the Cases h = 60.0 and 65.0 Å[a]

	h = 60.0 Å					h = 65.0 Å				
k	r_0 (Å)	R_2 (Å)	H (Å^{-1})	θ (deg)	ϵ (Å)	r_0 (Å)	R_2 (Å)	H (Å^{-1})	θ (deg)	ϵ (Å)
0.0	26.5	102.7	0.0237	104.0	0.04	26.2	98.0	0.0242	105.1	0.04
0.1	26.6	100.5	0.0238	104.3	0.04	26.0	88.2	0.0249	106.8	0.02
0.2	26.2	130.9	0.0229	100.8	0.03	25.5	134.2	0.0234	100.7	0.04
0.3	25.6	322.1	0.0211	94.3	0.04	24.8	270.2	0.0220	95.2	0.03
0.4	24.2	−190.2	0.0180	83.1	0.04	23.1	−226.5	0.0194	84.2	0.03
0.5	23.0	−66.8	0.0143	71.2	0.03	21.8	−67.0	0.0155	71.5	0.03
0.6	20.0	−29.1	0.0079	49.5	0.04	18.2	−28.5	0.0100	50.8	0.03
0.65	16.2	−18.9	0.0043	33.2	0.06	*	*	*	*	*
0.66	15.2	−17.0	0.0035	29.0	0.08	–	–	–	–	–
0.67	14.0	−15.4	0.0032	26.1	0.08	–	–	–	–	–

[a]AS bridges that remain asymmetric during all simulation times are indicated by an asterisk.

able to calculate the theoretical values for the volume Ω, and the areas of liquid−gas A_{LG} and liquid−solid A_{LS} interfaces.

IV. RESULTS

We present our results in two separate sections. In section IV.A, we discuss the AS bridges before their rupture occur. This includes the stable AS bridges ($h \leq h_S$) that do not break during the whole simulation time Δt_{sim}, and unstable AS bridges at the rupture walls separation ($h = h_C$ and $h_{C'}$) that break, but only after a sufficiently long time window that allows for the calculation of the profile of AS bridge and the forces/pressures on the walls. We consider all surface polarities $0 \leq k \leq 0.67$; values of h are in the range 50 to 75 Å. The aim of section IV.A is to compare the predictions of CT (e.g., profile of AS bridge and force induced on the walls) with the results from MD simulations. This study explores new aspects of the nanoscale AS bridge, which were not shown in our previous work,[2] where CT predictions were confirmed for nanoscale droplets and bridges at fixed h = 50 Å. The AS bridges of ref 2 are at least 4 nm-thick. By increasing h, we are able to test CT to even smaller scales. We find that CT holds for all the AS bridges studied here. This is remarkable given the small dimensions of the AS bridges, for example, the neck radius can be as small as $r_0 \approx 1$ nm, approximately three water molecules in length.

In section IV.B, we focus on the AS bridge rupture at the critical heights $h = h_C$ and $h_{C'}$, such that $h_S < h_C$ and $h_{C'}$, for all surfaces studied. Specifically, we compare the predictions of CT for the critical walls separation at which the AS bridge breaks ($h_{max,a}$ and $h_{max,s}$, see eqs 18, 19, and 21) with the corresponding values obtained from MD simulations (h_C and $h_{C'}$). We also study whether the AS bridges breaks into one or two (symmetric/asymmetric) droplets and how this rupture mechanism depends on the surface hydrophobicity/hydrophilicity. In particular, we test whether the results from MD are in agreement with CT. We find that the agreement between CT and simulations is, again, excellent.

IV.A. Profiles of Axisymmetric Bridges and Forces Induced on the Walls. CT predicts that stable AS bridges are symmetric relative to the origin, see Figure 1. Our MD simulations confirm that this is indeed the case for the nanoscale AS bridges in the stable domain, $h \leq h_S$. However, at the critical walls separations h_C and $h_{C'}$, the AS bridges evolve with time and, depending on the surface polarity, they may become asymmetric. In these cases, we report the properties of the AS bridges as a function of time for $t < \tau_r$.

The profiles of AS bridges obtained from MD simulations $r_{prof}(z)$, for selected hydrophobic/hydrophilic surfaces (k = 0.0, 0.4, 0.5, and 0.66) are shown in Figure 2a−d (the profiles for all the surface polarities studied are presented in the Figure S1 of the Supporting Information). Included in Figure 2a−d are the profiles from CT $r(z)$ eq 2 that fit the MD simulation results. The agreement between CT and MD simulations is remarkable for all surface hydrophobicity/hydrophilicity and walls separations. The best fitting parameters (H, r_0) used in eq 2 for all the surfaces studied are given in Tables 1−4. Table 5

DOI: 10.1021/acs.jpcc.7b08577
J. Phys. Chem. C 2018, 122, 1556−1569

Table 3. Same as Table 2 for the Cases h = 70.0 and 75.0 Å

	h = 70.0 Å					h = 75.0 Å				
k	r_0 (Å)	R_2 (Å)	H (Å^{-1})	θ (deg)	ϵ (Å)	r_0 (Å)	R_2 (Å)	H (Å^{-1})	θ (deg)	ϵ (Å)
0.0	25.5	85.5	0.0255	107.3	0.02	–	–	–	–	–
0.1	*	*	*	*	*	–	–	–	–	–
0.2	24.7	148.8	0.0236	99.5	0.04	24.4	122.1	0.0246	101.4	0.03
0.3	24.0	341.0	0.0223	94.0	0.04	*	*	*	*	*
0.4	22.4	−274.2	0.0205	85.3	0.03	*	*	*	*	*
0.5	20.4	−65.7	0.0169	71.9	0.03	*	*	*	*	*
0.6	14.3	−20.9	0.0112	47.5	0.06	9.6	−14.0	0.0162	54.7	0.05
0.65	–	–	–	–	–	–	–	–	–	–
0.66	–	–	–	–	–	–	–	–	–	–
0.67	–	–	–	–	–	–	–	–	–	–

Table 4. Same as Table 3 for the Cases h = 57.5, 58.75, 62.5, 67.5, 68.75, and 72.5 Å[a]

k	h (Å)	r_0 (Å)	R_2 (Å)	H (Å^{-1})	θ (deg)	ϵ (Å)
0.0	67.5	25.6	98.4	0.0246	104.9	0.02
0.1	67.5	25.9	120.3	0.0235	102.2	0.02
	68.75	*	*	*	*	*
0.2	72.5	24.9	114.5	0.0245	102.6	0.05
0.3	72.5	*	*	*	*	*
0.4	72.5	*	*	*	*	*
0.5	72.5	*	*	*	*	*
0.6	72.5	11.3	−16.1	0.0132	48.9	0.05
0.65	62.5	*	*	*	*	*
0.66	57.5	17.0	−17.9	0.0016	26.5	0.03
	58.75	*	*	*	*	*
0.67	57.5	15.8	−16.4	0.0011	22.8	0.03

[a]Note that for k = 0.1 (k = 0.66) there are two simulations for h = 67.5 and 68.75 Å (h = 57.5 and 58.75 Å).

Table 5. Properties of AS Bridges at the Critical Separations $h = h_{C'}$ and h_C Shown in Figure 8 and Figures S3 and S5 of the Supporting Information[a]

k	θ (deg)	h (Å)	$\Delta N_d/N$	τ_r (ps)
0.0	105.6	70.0	1.000	1234
		67.5	1.000	1575
0.1	104.8	70.0	1.000	1332
		68.75	1.000	367
0.2	100.8	75.0	1.000	881
		72.5	1.000	717
0.3	94.3	75.0	1.000	2094
		72.5	1.000	889
0.4	84.4	75.0	1.000	2514
		72.5	1.000	7284
0.5	70.8	75.0	0.873	1402
		72.5	0.909	4915
0.6	50.4	75.0	0.086	262
		72.5	0.004	500
0.65	32.8	65.0	0.124	334
		62.5	0.215	5687
0.66	28.3	60.0	0.048	3341
		58.75	0.409	9382
0.67	25.8	60.0	0.045	2159
		57.5	0.149	18617

[a]τ_r is the time at which the AS bridge breaks. $\Delta N_d/N$ quantifies the sizes of the droplets attached to the upper/lower walls after the bridge ruptures (see text).

includes the quantities relevant to the AS bridge rupture process, such as the rupture walls separation and the characteristic time τ_r, for all the surfaces considered. The unstable profiles included in Figure 2a–d and in Figure S1 of the Supporting Information correspond to the surfaces with polarities k and at walls separations h indicated in Table 5. Note that the quantities shown in each item of the Table 5 were obtained from single runs simulations, only relevant for this section.

From the fitting parameters shown in Tables 1–4, we can perform additional tests of CT at the nanoscale. Specifically, CT assumes that the contact angle θ of water depends solely on the surface hydrophobicity/hydrophilicity and hence, that it is independent of the AS bridge dimensions, such as the AS bridge height h. We confirm that this assumption holds for all AS bridges studied. Figure 3a shows that indeed θ is practically independent of h for all surfaces considered. The values of $\theta(h)$ deviate by no more than 3° to 4° from the corresponding average which is the typical uncertainty of contact angles measured in computer simulations of nanoscale droplets (see e.g., ref 33). The contact angles for all surface studied, averaged over h, are reported in Figure 3b. Our values of θ are in agreement with the corresponding values reported in our previous work[2] based on nanoscale droplets and capillary bridges in contact with the same surfaces considered here (in ref 2, h = 50 Å). Interestingly, we note that in the comparison of the profiles of AS bridges from CT and MD simulations we did not include any line tension. It follows that for the present nanoscale AS bridges, line tensions play a minor role (see also ref 2).

Knowledge of the theoretical profiles $r(z)$, defined by the fitting parameters (H, r_0) in Tables 1–4, allows us to calculate geometrical properties of the AS bridges, such as the areas of the liquid–solid and liquid–gas interfaces (A_{LS} and A_{LG}), and the volume Ω. These properties are shown in Figure 4a–c for all surfaces considered. A_{LS} and A_{LG} both vary as the AS bridge is stretched, and are in agreement with the prediction of CT given by eqs 10, 33, 8, and 28 of the Supporting Information. Interestingly, we find that the volume of all the AS bridges considered is rather constant. $\Omega(h)$ exhibits fluctuations for all surfaces studied, however, the standard deviation of Ω, sampled over all data, is 3.2% of its corresponding average; Table 6 shows the average of AS bridge volume for each k studied. We also calculate the surface free energy $\mathcal{F}$ for all cases studied and compare it with the predictions from CT. $\mathcal{F}$ can be calculated, using eq 11, from the geometry of the AS bridge, see Figures 4a and 4b, and the surface tension γ, which will be discussed ahead. The corresponding analytical expression from CT is

DOI: 10.1021/acs.jpcc.7b08577
J. Phys. Chem. C 2018, 122, 1556–1569

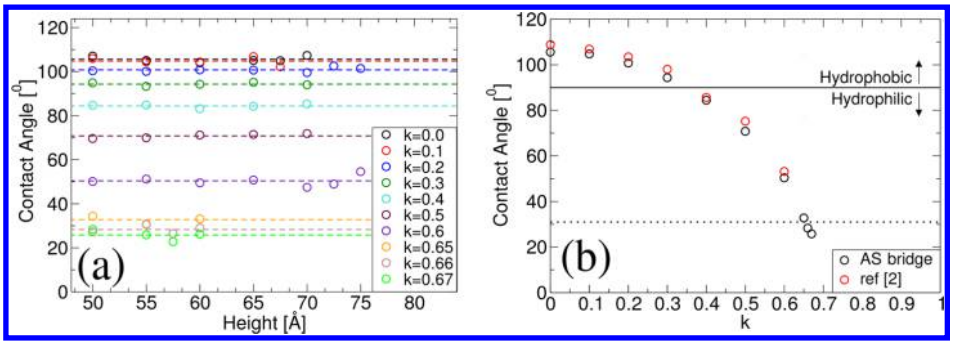

Figure 3. (a) Water contact angle $\theta(h)$ calculated from AS bridges formed between walls separated by a distance h, for all surface polarities k (see also Figure S1 of the Supporting Information). Error bars are smaller than the symbol size. The dashed lines are the contact angles averaged over h. (b) Contact angles averaged over h as a function of the surface polarity k. For comparison, we include the water contact angles from ref 2 (red circles) for the same surfaces considered here. Error bars are smaller than the symbol sizes. In part b, the black solid (dotted) line indicates $\theta = 90°$ ($\theta = 31°$).

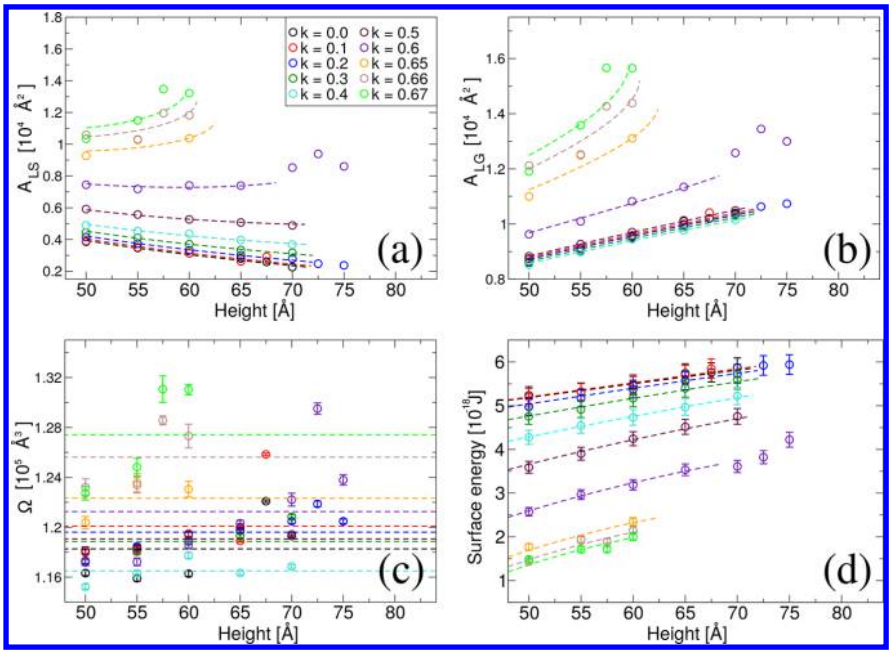

Figure 4. (a) Total liquid−solid interface area A_{LS} and (b) liquid−gas interface area A_{LG} of AS bridges formed between walls of surface polarity k as a function the walls separation h. (c) Volume Ω of AS bridges considered in parts a and b. (d) Surface free energy $\mathcal{F}$ calculated with eq 11 (circles) from results shown on panels a and b. The dashed lines in part c are the volumes averaged over h, see Table 6. The dashed lines in parts a, b, and d are the CT predictions given in eqs 10, 33, 8, 28, 6, and 34 of the Supporting Information. The error bars in parts a and b are smaller than the symbol size.

given in eq 16, and eqs 6 and 34 of the Supporting Information. The agreement between MD simulations and CT is excellent as shown in Figure 4d.

Next, we focus on the calculation of the force and pressure that the AS bridge exerts on the walls at different values of h and for all surface polarities k. The forces exerted on the walls by the AS bridge are calculated directly from our MD simulations. Specifically, during the MD simulations, we calculate the sum of the Coulomb and Lennard-Jones forces between all water molecules and all atoms that belong to each wall. We evaluate the components F_x, F_y, and F_z of the total force on each wall averaged over time. The time averages of F_x and F_y converge to zero for long times, as expected, and hence, their deviations from zero provide an estimation of the force error bars. In addition, due to the symmetry of the system, we average the normal components of the force acting on the two walls: $F_z = (\vec{F}_1 \cdot \check{n}_1 + \vec{F}_2 \cdot \check{n}_2)/2$, where $\vec{F}_i$ is the force acting on wall $i = 1, 2$ and $\check{n}_i$ is a unit vector perpendicular to wall i, pointing toward the AS bridge. It follows that if $F_z > 0$ ($F_z < 0$) then the AS bridge induces an effective atractive (repulsive) force between the walls. We note that, from the calculated F_z, we are able to measure other properties, such as the liquid−vapor surface tension of SPC/E water and the pressure inside the AS bridges.

We first calculate the liquid−vapor surface tension using the net forces obtained from MD simulations and the corresponding prediction from CT given in eq 7. Figure 5a shows the forces obtained from MD simulations, for all wall separations and surface polarities studied, as a function of the parameter $C(k)$. Our data clearly indicates that $F_z \propto C(k)$ (dashed line), in agreement with eq 7. Small deviations in the MD simulation data are present for surface polarities $k = 0.65$, 0.66, and 0.67. For these surface polarities, however, the AS bridges are close

DOI: 10.1021/acs.jpcc.7b08577
J. Phys. Chem. C 2018, 122, 1556−1569

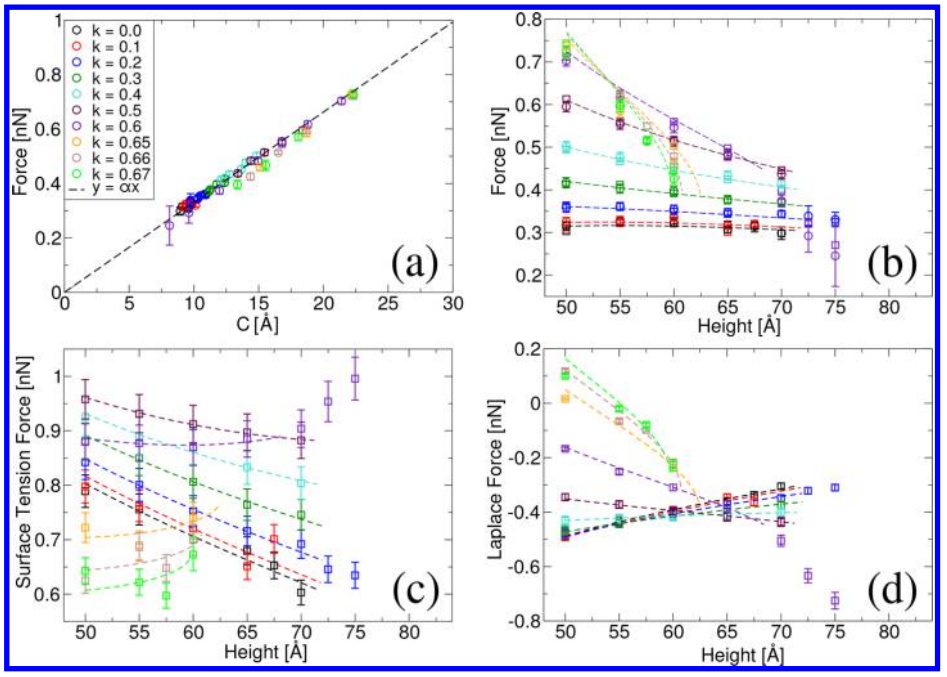

Figure 5. Forces induced by AS bridges formed between parallel walls as a function of (a) the neck parameter $C = r_0 - Hr_0^2$ (see eq 7) and (b) the walls separations h, for all surface polarities k. In part a, the dashed line is the best linear regression intercepting the origin ($y = \alpha x$) for $k < 0.65$ (see text). The slope of the line is $\alpha = 2\pi\gamma$ with $\gamma = 0.053 \pm 0.002$ N/m. In part b, the circles represent results from MD simulations; squares and dashed lines are, respectively, CT predictions from eq 7, and eqs 4 and 23 of the Supporting Information. The error bars on squares in part b are smaller than 0.02 nN. Panels c and d are, respectively, the contributions to the total force due to the liquid−vapor interface F_γ and Laplace pressure F_P. Squares and the dashed lines are, respectively, CT predictions given in eqs 4 and 5, and eqs 11, 25, 12, and 27 of the Supporting Information.

to their critical heights (i.e., h = 50 to 60 Å, and h_C and $h_{C'} \approx 60$ Å).

Equation 7 indicates that the slope of the dashed line in Figure 5a should be $2\pi\gamma$. Using this expression we obtain $\gamma = 0.053 \pm 0.002$ N/m. This value of γ is consistent with the values of the liquid−vapor surface tension of SPC/E water available in the literature[34,35] and it is also in agreement with the value of γ calculated independently using the Kirkwood-Buff method.[2]

A more detailed comparison of the forces calculated from MD simulations and CT is included in Figure 5b where F_z is shown as a function of h. We include the predictions from CT given in eqs 7 and 14 and eqs 4 and 23 of the Supporting Information. Since that $F_z = F_{z,neck}$ for stable AS bridge, we plot $F_{z,neck}$ given by eq 7. This is important since eq 7 requires only access to the parameters (H, r_0) of Tables 1−4. Instead, eq 14 and eqs 4 and 23 of the Supporting Information require the calculation of Ω and θ, and they are based on elliptical integrals. The results of Figure 5b clearly show that the expressions from CT eqs 7 and 14, and eqs 4 and 23 of the Supporting Information are equivalent, as one would heave expected. In particular, they are consistent with the results from MD simulations. Therefore, it follows that CT is able to predict not only the geometry of nanoscale AS bridges, but their thermodynamic properties, such as the forces on the walls. Again, we note that our nanoscale AS bridges are surprisingly small, with neck radii as small as ≈10 Å. For comparison, we note that the typical thickness of the water-vapor interface (at $T \approx 300$ K) is ≥8−10 Å,[36,37] i.e., comparable to the minimum values of r_0 for the studied AS bridges.

The force on the walls is the sum of the force produced by the liquid−vapor interface of the AS bridge eq 4) and the force due to the Laplace pressure within the AS bridge (Laplace force, eq 5. F_γ and F_P are shown in Figures 5, parts c and d, respectively, for all h and walls studied. While F_γ is always positive, as predicted by eq 4, F_P can be either positive or negative, see eq 5. In other words, F_γ always induces an effective attraction between the walls. Instead, F_P induces an effective attraction between the walls only for surface polarities $k \geq 0.65$ and approximately h < 50 to 55 Å; otherwise, F_P is repulsive, independently of the surface hydophobicity/hydrophilicity. It is obvious, however, that for small enough wall separation, F_P will become attractive for hydrophilic walls.

We note that Figures 5, parts c and d include, respectively, the prediction from CT for F_γ eq 4 and F_P eq 5 evaluated by two different approaches. In one case (squares), we calculate r_b from the theoretical profile defined by the parameters (H, r_0) given in Tables 1−4. In the second approach, r_b is obtained from eqs 9 and 24 of the Supporting Information which follows by evaluating elliptical integrals (dashed lines). In all cases of parts b−d of Figure 5, we show the value of the resultant force and its components up to the maximum height at which the AS bridges are expected to be stable, and the numerical and analytical approach provide consistent values for F_γ, F_P, and the net force F_z.

We conclude this section by discussing the Laplace pressure within the AS bridges. Figure 6 shows P as a function of h and for all surface polarities k studied. The Laplace pressure is calculated from MD simulations (circles) using eq 9. Specifically, we use eq 9 with F_z obtained directly from MD simulations, as explained above, and r_b being calculated from the theoretical profile of the AS bridge using the parameters of Tables 1−4. We compare the MD simulation values of P with the corresponding theoretical values. The CT predictions are obtained from two different approaches. In one case, P is calculated from the Young−Laplace eq 1, considering that the

DOI: 10.1021/acs.jpcc.7b08577
J. Phys. Chem. C 2018, 122, 1556−1569

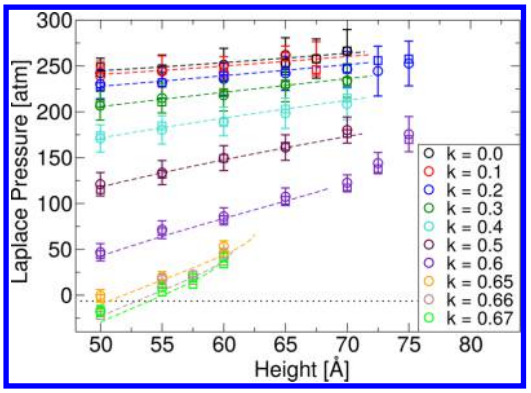

Figure 6. Laplace pressure inside the AS bridges as a function of the surface polarity k and walls separation h. Squares and circles are, respectively, the Laplace pressure calculated from eqs 1 and 9. The error bars on squares are smaller than 10 atm. The dashed lines are the closed-form expression of CT given in eq 15 and eqs 5 and 26 of the Supporting Information.

pressure outside the water AS bridge is equal to zero and using the value of H from Tables 1−4 (crosses). In the second approach, we use the CT expression given in eq 15, and eqs 5 and 26 of the Supporting Information, based on elliptical integrals (dashed lines). In both cases, we use $\gamma = 0.053 \pm 0.002$ N/m. As expected, the pressure calculated following both approached are consistent with one another, validating both methods.

Figure 6 shows a remarkable agreement between CT and MD simulations. One of the most interesting result from this figure is that P can be negative, a behavior not found in macroscale capillary bridges. This is due to the very small values of the neck radius accessible in nanoscale AS bridges which determine the sign of H in Young−Laplace eq 1. Interesting, the range of P in Figure 6 is very large, expanding to ≈275 atm. In particular, we note that stretching an AS bridge can lead to a considerable increase in Laplace pressure, independently of the surface hydrophobicity/hydrophilicity. For example, in the case of $k = 0.6$, P increases by roughly 100% when h varies from 5 to 7 nm.

IV.B. Rupture Mechanism and Limit of Stability of Axisymmetric Bridges. In this section, we analyze the behavior of AS bridges at the critical walls separation during their rupture. Parts a−d of Figure 7 show, respectively, the time evolution of the AS bridges in contact with surfaces of polarity $k = 0.0$, 0.4, 0.5, and 0.66 at $h = h_{C'}$ (the figures for all the surface polarities studied at $h = h_C$ and $h_{C'}$, are included in Figures S2 and S4 of the Supporting Information). Each line in the panels of Figure 7 represents one profile of AS bridge averaged of 0.1 ns (see section III.B.1) and the gradient color, from blue to magenta, shows the evolution of the AS bridge with time. The AS bridges evolve monotonically with time and their rupture is rather fast. The AS bridges break into a single droplet attached to one of the walls for $k \leq 0.4$ and they split into two droplets, one attached to each wall, for $k > 0.4$. Interestingly, $\theta \approx 85°$ for $k = 0.4$ which is close to the critical value $\theta = 90°$ for $k \approx 0.37$ (see Figure 3b). Snapshots of the AS bridges at the rupture time τ_r, for the surface polarity discussed here, are shown in parts a−d of Figure 8 (snapshots at time τ_r for all the surface polarities studied and $h = h_C$ and $h_{C'}$ are included in Figures S3 and S5 of the Supporting Information).

As discussed in section II.B, CT predicts that AS bridges should break into two identical droplets for contact angles $\theta < 31°$. Next, we test whether our MD simulations are in agreement with this prediction. We estimate the volume of each droplet by counting the number of water molecules at $t = \tau_r$ (see Figure 8) that are above and below the empty gap. We report $|\Delta N_d|/N$, where ΔN_d is the difference in the number of

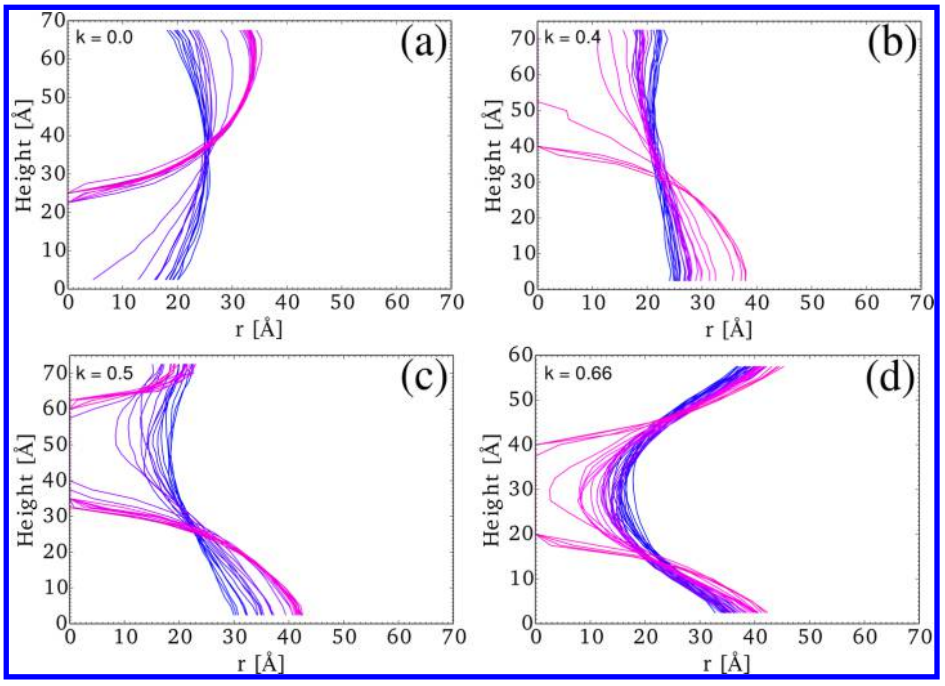

Figure 7. Profiles of AS bridges during the rupture at the critical walls separation $h_{C'}$. Each profile is obtained over a time window of 0.1 ns, and the gradient color indicates the time evolution of the AS bridge; time increases from blue to magenta profiles. Additional AS bridge profiles showing the rupture at the critical height $h_{C'}$ and h_C, for the other values of k studied, are included in Figures S2 and S4 of the Supporting Information, respectively.

DOI: 10.1021/acs.jpcc.7b08577
J. Phys. Chem. C 2018, 122, 1556−1569

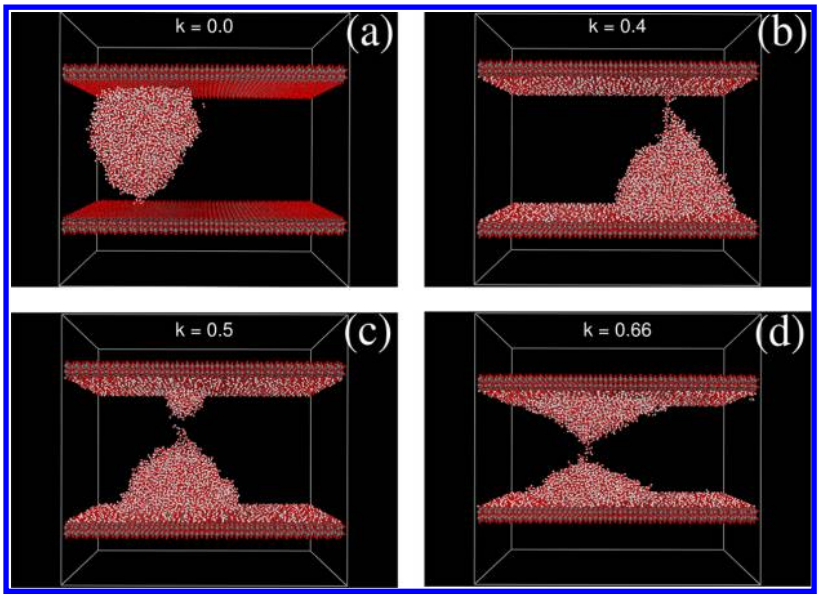

Figure 8. Snapshots of AS bridges at the critical height $h_{C'}$ and rupture time τ_r. Hydrogen on the walls are removed in panel (a) since they have no effective interactions with other atoms. The contact angle in part d is $\theta = 28.9° < 31°$ and, in agreement with CT, the bridge ruptures leading to two symmetric droplets, one on each wall. Additional snapshots of AS bridge at the critical height $h_{C'}$ and h_C, for the other values of k studied, are included in Figures S3 and S5 of the Supporting Information, respectively.

water molecules of the droplets. It follows that $0 \leq |\Delta N_d|/N \leq 1$ and that the AS bridge breaks into a single droplet for $|\Delta N_d|/N = 1$ while $|\Delta N_d|/N = 0$ if the AS bridge breaks into two identical droplets (symmetric rupture). The Table 5 includes the calculated $|\Delta N_d|/N$ for all configurations shown in Figures 8a–d and Figures S3 and S5 of the Supporting Information. The Figure 9 shows the average of $|\Delta N_d|/N$ as a function of θ,

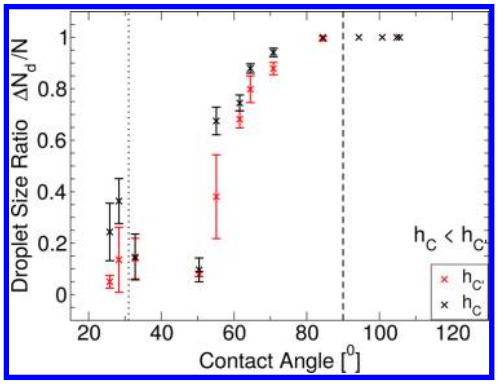

Figure 9. Droplet size ratio $\Delta N_d/N$ formed after the rupture of AS bridge, as a function of the contact angle θ. The AS bridge breaks into a single droplet for $\Delta N_d/N = 1$, while $\Delta N_d/N = 0$ if the AS bridge breaks into two identical droplets. Values of $\theta = 55.1°$, 61.6°, and 64.5° are obtained from the surface polarity $k = 0.576$, 0.553, and 0.527, respectively. The error bars are calculated over 5–10 independent MD simulations. The AS bridges break into two symmetrical droplets for approximately $\theta < 45°$.

and the results from MD simulations are close to the CT predictions. Specifically, MD simulations indicate that $|\Delta N_d|/N \approx 0$ for approximately $\theta < 45°$.

Next, we compare the critical height obtained from MD simulations (h_C and $h_{C'}$) with the corresponding prediction from CT. Figure 10 shows the maximum normalized stable height $h_{max,a}$ (solid line) and metastable height $h_{max,s}$ (dashed-dotted line) obtained from CT using eqs 18, 19, and 21, and

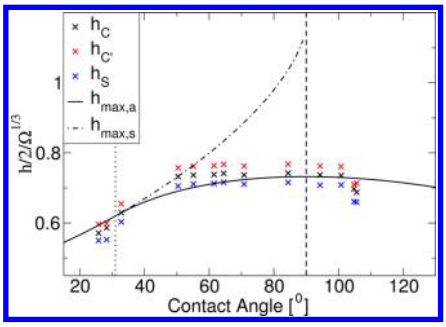

Figure 10. Maximum walls separation h_S at which the AS bridge remain stable during the MD simulations, and the corresponding critical separations h_C and $h_{C'}$ at which the AS bridges break (see text). h_S, h_C, and $h_{C'}$ are normalized by $2\,\Omega^{1/3}$, where Ω is the average bridge volume (see Table 6). $h_{max,a}$ (solid line) and $h_{max,s}$ (dashed-dotted line) are the predictions of CT obtained from eqs 18, and 21, and 19, respectively. The vertical dotted line shows the critical contact angle 31° bellow which the AS bridge is predicted to break into two symmetric droplets. The vertical dashed line shows the contact angle 90°, which is the separation between hydrophilic and hydrophobic surfaces.

the critical heights $h_{C'}$ and h_C obtained from MD simulations (crosses), based on the AS bridge volume averaged over all values of h; see Table 6. For comparison, we also include $h_S/(2\Omega^{1/3})$. The main point of Figure 10 is that there is an agreement between CT theory and MD simulations. In particular, the MD simulations results show that the AS bridges break near the $h_{max,a}$, i.e., at the limit of stability predicted by CT. In these cases, the CT predicts that the AS bridges are asymmetric ($z_0 \neq 0$) before the rupture.

Similar results were obtained in ref 10 in which the simulations of the AS bridge rupture were performed using Kawasaki dynamics on a lattice-gas model. In agreement with ref 10, we observe that the critical heights $h = h_C, h_{C'}$ follows eq 19, which describes the symmetric rupture for $\theta > 31°$ and hence, exceeding the range of validity predicted by CT ($\theta <$

DOI: 10.1021/acs.jpcc.7b08577
J. Phys. Chem. C 2018, 122, 1556–1569

Table 6. Average of Contact Angles θ and Volumes Ω of AS Bridges as a Function of the Surface Polarity k Obtained from the Profiles $r(z)$ Shown in Figures 2a–d and Figure S1 of the Supporting Information

k	θ (deg)	Ω (Å^3)
0.0	105.6	118264.8
0.1	104.8	120076.0
0.2	100.8	119603.8
0.3	94.3	118866.0
0.4	84.4	116493.9
0.5	70.8	119066.1
0.6	50.4	121256.0
0.65	32.8	122326.4
0.66	28.3	125617.5
0.67	25.8	127405.2

31°). This fact can be explained by the difference in dynamics for symmetric and asymmetric ruptures. The asymmetric rupture involves global flow of the viscous fluid from the smaller droplet to the larger one through a narrow neck. This is a slow process which may take much longer than our simulations time Δt_{sim} at a given h. Thus, during the stretching process, the AS bridge continues to exist until h reaches the value predicted by symmetric rupture which involves only local displacement of fluid near the neck, and thus takes much smaller time, which is comparable with the simulation time step used to increase h. Thus, simulated rupture happens approximately at the walls separation predicted by the symmetric rupture, eq 19, at which the AS bridge becomes unstable with respect to symmetric fluctuations.

Fluctuations are expected to play a relevant role at the nanoscale. In the case of AS bridges, one may expect that fluctuations in the profile of AS bridge may become more pronounced as the critical walls separation is approached. In order to test for the presence of fluctuations on the profiles of AS bridges as h increases, we calculate the average position of the AS bridge neck, z_0, as a function of h; see Figure 11. Interestingly, we find that the behavior of z_0 with increasing h depends on the hydophobicity/hydrophilicity of the surface, which affects the convergence of z_0. Specifically, for hydrophilic surfaces with polarity k = 0.65 to 0.67, $z_0(h) \sim 0 \pm 5$ Å. At these surface polarities, the AS bridge breaks into 2 identical droplets and hence, z_0 barely fluctuates as the critical walls separation is approached. Instead, for hydrophobic surfaces, e.g. k = 0.1, $z_0(h) \sim 0 \pm 5$ Å only for h < 65 Å. As the critical walls separation is approached, these AS bridges break leading to a single droplet on one of the walls, and hence, $z_0(h)$ fluctuates considerably with increasing h; for example, the case h = 70 Å and k = 0.4 does not converges for 15 ns simulation.

V. SUMMARY

In this work, we confirm the validity of continuum theory of capillarity at the nanoscale by performing computer simulations of water AS bridges. The AS bridges studied are placed between two identical β-cristobalite based walls with different degrees of hydrophilicity/hydrophobicity. By increasing the separation between the walls, we are able to sweep the AS bridge phase diagram, and test the predictions of CT for small equilibrium AS bridges, with dimensions down to ~2 nm in thickness, which is comparable to the thickness of the vapor liquid interface (~0.5 to 0.8 nm). The predictions of CT are also

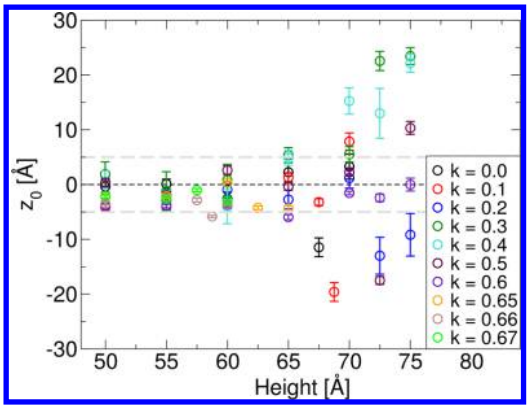

Figure 11. Average distance of the location z_0 of AS bridge neck, relative to the midpoint between the walls (z = 0 in Figure 1b), for all surfaces and wall separations studied. z_0 converges to 0, however it may be slow depending on fluctuations, which depends on h and k. Gray dashed lines indicate $z_0 = \pm 5$ Å. The data within (outside) the region of ±5 Å are stable (unstable) AS bridges. Note that the case h = 70 Å and k = 0.4 does not converges for 15 ns simulation. For $k \geqslant 0.6$, $-5 \leq z_0 \leq 5$ Å, i.e., it shows small fluctuations, and the AS bridge ruptures into two droplets with similar volume (symmetric rupture). For $k < 0.6$, z_0 can fluctuate considerably and the AS bridge ruptures into either one droplet or two droplets of different size (asymmetric rupture).

tested during the AS bridge rupture at wall separations for which the AS bridges become unstable.

In the first part of this work, we study the properties of AS bridges in the stable region of the phase diagram (θ, h) ($h_S < h_{max,a}$), i.e., during the stretching process before the AS bridges rupture occurred. We show that the geometrical properties of the AS bridges obtained from MD simulations, such as the average profile, contact angle, neck radius, curvature, and volume were in excellent agreement with CT. This agreement is found to hold for all surfaces studied and does not require the introduction of line tensions. Thermodynamic properties such as surface tension, surface free energy, Laplace pressure and the capillary adhesion force induced by the AS bridges on the walls are also studied. Again, for all surfaces considered, the agreement between CT and MD simulations is remarkable.

In the second part of this work, we study the AS bridges in the unstable region of phase diagram (θ, h) ($h > h_S$), where the rupture process occurs. We find that the critical wall separation at which the AS bridges break ($h_{C'}$ and h_C) is in good agreement with the critical heights predicted by CT ($h_{max,a}$ and $h_{max,s}$). In addition, consistent with macroscopic CT, MD simulations show that the AS bridge could break into one or two droplets, of same or different size, depending on the contact angle of water. We observe that for $\theta > 84.4°$, close to the value 90° predicted by CT, the AS bridge forms a single droplet after its rupture. For $\theta < 45°$ we observe the formation of droplets approximately symmetrical. For θ = 28.3° we observe the formation of two droplets of different size, one next to each wall (asymmetrical rupture). With our current data, it is not possible to fully understand the small discrepancy from the CT prediction and our data, which could be a subject for a different work.

The present study is a strong test of the validity of capillarity theory at the nanoscale. This work indicates that CT is still a useful tool to describe capillary phenomena at the nanoscale, where atomistic details can be relevant, including complex processes such as the rupture of AS bridges. The phase diagram

DOI: 10.1021/acs.jpcc.7b08577
J. Phys. Chem. C 2018, 122, 1556–1569

we explored here is of practical relevance, for example, to improve ink-transfer processes in dip-pen nanolithography[15] and for improvement of AFM measurements.[38] Our studies also provides simple methodologies to compare the complex mathematical expression of CT and results from MD simulations.

■ ASSOCIATED CONTENT

Supporting Information

The Supporting Information is available free of charge on the ACS Publications website at DOI: 10.1021/acs.jpcc.7b08577.

The Supporting Information provides the analytical expressions of F_z, P, and $\mathcal{F}$, and the complete set of figures which complements Figures 2, 7, and 8 (PDF)

■ AUTHOR INFORMATION

Corresponding Author

*(A.M.A.) E-mail: aalencar@usp.br.

ORCID

Alexandre B. Almeida: 0000-0002-8042-4844

Adriano M. Alencar: 0000-0001-9324-2698

Notes

The authors declare no competing financial interest.

■ ACKNOWLEDGMENTS

This research was supported by the National Council for Scientific and Technological Development (CNPq−465259/2014-6), the Coordination for the Improvement of Higher Education Personnel (CAPES−BEX 5179/14-9), the National Institute of Science and Technology Complex Fluids (INCT-FCx), and the São Paulo Research Foundation (FAPESP−2014/50983-3 and 2014/22102-2). N.G. was supported by the National Science Foundation under Grant No. CBET-1604504, by a grant of computer time from the City University of New York High Performance Computing Center under NSF Grants CNS-0855217, CNS-0958379 and ACI-1126113, and by a PSC−CUNY Award, jointly funded by The Professional Staff Congress and The City University of New York. S.V.B. thanks the Dr. Bernard W. Gamson Computational Science Center at Yeshiva College for support.

■ REFERENCES

(1) de Gennes, P.; Brochard-Wyart, F.; Quéré, D. *Capillarity and Wetting Phenomena: Drops, Bubbles, Pearls, Waves*; Springer: 2004.

(2) Giovambattista, N.; Almeida, A. B.; Alencar, A. M.; Buldyrev, S. V. Validation of Capillarity Theory at the Nanometer Scale by Atomistic Computer Simulations of Water Droplets and Bridges in Contact with Hydrophobic and Hydrophilic Surfaces. *J. Phys. Chem. C* **2016**, *120*, 1597−1608.

(3) Langbein, D. *Capillary Surfaces: Shape-Stability-Dynamics, in Particular under Weightlessness*; Springer: 2002.

(4) Heady, R. B.; Cahn, J. W. An Analysis of the Capillary Forces in Liquid-Phase Sintering of Spherical Particles. *Metall. Mater. Trans. B* **1970**, *1*, 185−189.

(5) Niven, R. K. Force Stability of Pore-Scale Fluid Bridges and Ganglia in Axisymmetric and Non-axisymmetric Configurations. *J. Pet. Sci. Eng.* **2006**, *52*, 1−18.

(6) Alencar, A. M.; Arold, S. P.; Majumdar, A.; Stamenovic, D.; Stanley, H. E.; Suki, B.; et al. Dynamic Instabilities in the Inflating Lung. *Nature* **2002**, *417*, 809−811.

(7) Suki, B.; Alencar, A. M.; Tolnai, J.; Asztalos, T.; Petak, F.; Sujeer, M. K.; Patel, K.; Stanley, H. E.; Hantos, Z.; et al. Size Distribution of Recruited Alveolar Volumes in Airway Reopening. *J. Appl. Physiol.* **2000**, *89*, 2030−2040.

(8) Alencar, A. M.; Majumdar, A.; Hantos, Z.; Buldyrev, S. V.; Stanley, H. E.; Suki, B. Crackles and Instabilities During Lung Inflation. *Phys. A* **2005**, *357*, 18−26.

(9) Alencar, A. M.; Buldyrev, S. V.; Majumdar, A.; Stanley, H. E.; Suki, B. Avalanche Dynamics of Crackle Sound. *Phys. Rev. Lett.* **2001**, *87*, 088101.

(10) Alencar, A. M.; Wolfe, E.; Buldyrev, S. V. Monte Carlo Simulation of Liquid Bridge Rupture: Application to Lung Physiology. *Phys. Rev. E* **2006**, *74*, 026311.

(11) Almeida, A. B.; Buldyrev, S. V.; Alencar, A. M. Crackling Sound Generation During the Formation of Liquid Bridges: A Lattice Gas Model. *Phys. A* **2013**, *392*, 3409−3416.

(12) van Honschoten, J. W.; Brunets, N.; Tas, N. R. Capillarity at the Nanoscale. *Chem. Soc. Rev.* **2010**, *39*, 1096−1114.

(13) Gravelle, S.; Ybert, C.; Bocquet, L.; Joly, L. Anomalous Capillary Filling and Wettability Reversal in Nanochannels. *Phys. Rev. E: Stat. Phys., Plasmas, Fluids, Relat. Interdiscip. Top.* **2016**, *93*, 033123.

(14) Kelly, S.; Torres-Verdín, C.; Balhoff, M. T. Anomalous Liquid Imbibition at the Nanoscale: the Critical Role of Interfacial Deformations. *Nanoscale* **2016**, *8*, 2751−2767.

(15) Eichelsdoerfer, D. J.; Brown, K. A.; Mirkin, C. A. Capillary Bridge Rupture in Dip-pen Nanolithography. *Soft Matter* **2014**, *10*, 5603−5608.

(16) Yang, L.; Tu, Y.-s.; Tan, H.-l Influence of Atomic Force Microscope (AFM) Probe Shape on Adhesion Force Measured in Humidity Environment. *Environment. Appl. Math. Mech. -ENGL* **2014**, *35*, 567−574.

(17) Weeks, B. L.; Vaughn, M. W.; DeYoreo, J. J. Direct Imaging of Meniscus Formation in Atomic Force Microscopy Using Environmental Scanning Electron Microscopy. *Langmuir* **2005**, *21*, 8096−8098.

(18) Kralchevsky, P. A.; Denkov, N. D. Capillary Forces and Structuring in Layers of Colloid Particles. *Curr. Opin. Colloid Interface Sci.* **2001**, *6*, 383−401.

(19) Laube, J.; Dörmann, M.; Schmid, H. J.; Mädler, L.; Colombi Ciacchi, L. Dependencies of the Adhesion Forces between TiO_2 Nanoparticles on Size and Ambient Humidity. *J. Phys. Chem. C* **2017**, *121*, 15294−15303.

(20) Cheng, S.; Robbins, M. O. Capillary Adhesion at the Nanometer Scale. *Phys. Rev. E* **2014**, *89*, 062402.

(21) Valenzuela, G. E.; Saavedra, J. H.; Rozas, R. E.; Toledo, P. G. Force Exerted by a Nanoscale Capillary Water Bridge Between Two Planar Substrates. *Phys. Chem. Chem. Phys.* **2016**, *18*, 11176−11183.

(22) Bak, W.; Sung, B.; Kim, J.; Kwon, S.; Kim, B.; Jhe, W. Time-Resolved Observation of Thermally Activated Rupture of a Capillary-Condensed Water Nanobridge. *Appl. Phys. Lett.* **2015**, *106*, 013102.

(23) Men, Y.; Zhang, X.; Wang, W. Capillary Liquid Bridges in Atomic Force Microscopy: Formation, Rupture, and Hysteresis. *J. Chem. Phys.* **2009**, *131*, 184702.

(24) Vogel, T. I. Stability of a Liquid Drop Trapped Between Two Parallel Planes. *SIAM J. Appl. Math.* **1987**, *47*, 516−525.

(25) Vogel, T. I. Stability of a Liquid Drop Trapped Between Two Parallel Planes II: General Contact Angles. *SIAM J. Appl. Math.* **1989**, *49*, 1009−1028.

(26) Athanassenas, M. A Variational Problem for Constant Mean Curvature Surfaces with Free Boundary. *J. Reine Angew. Math.* **1987**, *377*, 97−107.

(27) Zhou, L. On Stability of a Catenoidal Liquid Bridge. *Pac. J. Math* **1997**, *178*, 185−198.

(28) Plimpton, S. Fast Parallel Algorithms for Short-Range Molecular Dynamics. *J. Comput. Phys.* **1995**, *117*, 1−19.

(29) Berendsen, H. J. C.; Grigera, J. R.; Straatsma, T. P. The Missing Term in Effective Pair Potentials. *J. Phys. Chem.* **1987**, *91*, 6269−6271.

(30) Hockney, R. W.; Eastwood, J. W. *Computer Simulation Using Particles*; Adam Hilger: New York, 1989.

(31) Giovambattista, N.; Rossky, P. J.; Debenedetti, P. G. Effect of Pressure on the Phase Behavior and Structure of Water Confined

Between Nanoscale Hydrophobic and Hydrophilic Plates. *Phys. Rev. E* **2006**, *73*, 041604.
(32) Giovambattista, N.; Debenedetti, P. G.; Rossky, P. J. Effect of Surface Polarity on Water Contact Angle and Interfacial Hydration Structure. *J. Phys. Chem. B* **2007**, *111*, 9581−9587.
(33) Wang, J.; Bratko, D.; Luzar, A. Probing Surface Tension Additivity on Chemically Heterogeneous Surfaces by a Molecular Approach. *Proc. Natl. Acad. Sci. U. S. A.* **2011**, *108*, 6374−6379.
(34) Vega, C.; de Miguel, E. Surface Tension of the Most Popular Models of Water by Using the Test-Area Simulation Method. *J. Chem. Phys.* **2007**, *126*, 154707.
(35) Ismail, A. E.; Grest, G. S.; Stevens, M. J. Capillary Waves at the Liquid-Vapor Interface and the Surface Tension of Water. *J. Chem. Phys.* **2006**, *125*, 014702.
(36) Romero-Vargas Castrillón, S.; Giovambattista, N.; Aksay, I. A.; Debenedetti, P. G. Structure and Energetics of Thin Film Water. *J. Phys. Chem. C* **2011**, *115*, 4624−4635.
(37) Willard, A. P.; Chandler, D. Instantaneous Liquid Interfaces. *J. Phys. Chem. B* **2010**, *114*, 1954−1958.
(38) Proksch, R.; Kocun, M.; Hurley, D.; Viani, M.; Labuda, A.; Meinhold, W.; Bemis, J. Practical Loss Tangent Imaging with Amplitude-Modulated Atomic Force Microscopy. *J. Appl. Phys.* **2016**, *119*, 134901.

DOI: 10.1021/acs.jpcc.7b08577
J. Phys. Chem. C 2018, 122, 1556−1569